

Article

Scaling Laws of Scheduling Gain for Uplink Massive MIMO Systems: Is User Scheduling Still Beneficial for Massive MIMO?

Taehyoung Kim ¹ and Sangjoon Park ^{2,*}

¹ Samsung Research, Samsung Electronics Company Ltd., Seoul 06765, Korea; khotdog86@gmail.com

² Department of Electronic Engineering, Kyonggi University, Suwon 16227, Korea

* Correspondence: sj.park@kgu.ac.kr; Tel.: +82-31-249-9798

Received: 11 September 2020; Accepted: 30 September 2020; Published: 10 October 2020



Abstract: In this paper, the scaling laws of scheduling gain and the feasibility of user scheduling for uplink massive multiple input–multiple output (MIMO) systems are investigated by analyzing the second moment of mutual information. We consider two well-known linear receivers of matched filter (MF) and zero-forcing (ZF). The exact distribution of the signal-to-interference-plus-noise ratio (SINR) and its moment-generating function are first obtained, and the approximated variance of the mutual information for a user is derived as a closed form with a function of the number of antennas. The achievable scheduling gain under the optimal user scheduler is then derived using the Gaussianity of the sum rate. From the analyses and simulation results, it is found that the scheduling gain for the MF receiver increases with the number of base station (BS) antennas, while that for the ZF receiver decreases as the number of BS antennas increases, for most cases (except some impractical scenarios). Therefore, it is verified that user scheduling is still beneficial for the MF receiver while random user selection is sufficient for the ZF receiver in massive MIMO systems.

Keywords: massive MIMO; user scheduling; matched filter; zero-forcing

1. Introduction

Recently, the fifth-generation (5G) wireless communication system, known as new radio (NR), has been successfully commercialized globally. With the development of 5G NR, the performance and functionality of cellular mobile communications have reached an unprecedented level [1]. Compared to the fourth-generation (4G) long-term evolution (LTE), the NR supports faster data rates, lower latency, higher reliability, and new spectrum bands for enabling a wide range of use cases, such as enhanced mobile broadband (eMBB), ultra-reliable low-latency communications (URLLC), and massive machine-type communications (mMTC) [2,3].

Massive multiple input–multiple output (MIMO), in which the base station (BS) is equipped with a few hundreds of antenna arrays, is a key feature for 5G NR, used to satisfy the target data rate requirement [4]. With the emerging large number of antennas, many users can be served simultaneously using given time and frequency resources through multiuser MIMO [5], which can significantly improve the spectral efficiency [6]. In addition to the capacity enhancement, massive MIMO has several benefits, such as the mitigation of uncorrelated noise and small-scale fading [7], high energy efficiency [8], low computational complexity for signal processing [9], and robustness against severe propagation loss and blockage in high-frequency ranges [10,11].

To further improve the achievable sum rate in massive MIMO systems, a proper user scheduling algorithm is typically employed in wireless communication systems [4], which selects the number of users to be served simultaneously in a spatial multiplexing manner. Therefore, many studies

have recently been conducted to investigate the user scheduling algorithm for various massive MIMO systems [12]. In [13], a semi-orthogonal user selection (SUS) algorithm was proposed for zero-forcing (ZF) precoding. In [14], a signal-to-interference-ratio-based user scheduling (SIRUS) method was addressed for matched filter (MF) precoding in downlink MIMO systems. For uplink massive MIMO, a multi-user grouping-based scheduling algorithm was investigated in [15], while a joint user scheduling and beam selection scheme was studied in [16] for beam-based massive MIMO systems. In [17], a greedy user selection algorithm for distributed massive MIMO was investigated. The aforementioned studies focused on reducing the complexity of optimal user scheduling, in which the complexity increased exponentially with the number of served users due to the exhaustive search.

Therefore, this study investigates whether user scheduling is necessary for massive MIMO systems. Many previous studies [7,18–20] have analyzed the performance of massive MIMO systems in terms of the ergodic sum rate. The optimality of MF was proven in [7] under the framework of non-cooperative multicellular networks. In [18], the deterministic equivalent forms of signal-to-interference-plus-noise ratio (SINR) for ZF and minimum mean-square error (MMSE) precoders were derived. In [19], the authors derived the asymptotic achievable rates of MF and MMSE precoders/receivers while considering pilot contamination. The effect of channel aging was analyzed in [20] using a similar analysis technique as that given in [18] and [19]. The previous works in [7,18–20] have studied the performance of massive MIMO systems regarding the first moment of mutual information. However, because the diversity gain from user scheduling depends on natural or artificially induced fluctuations in the channel, it is important to estimate the fluctuations that can be expected in a particular system environment to investigate the feasibility of user scheduling. Therefore, in this paper, the performance of a massive MIMO system is analyzed in terms of the second moment of mutual information (i.e., the variance of mutual information) to understand how the fluctuations in mutual information can be varied according to the number of antennas.

In [21–23], a phenomenon of massive MIMO systems, referred to as the channel hardening effect, was investigated. The channel hardening effect implies that the variance of mutual information shrinks as the number of antennas increases. In [21], the authors used Gaussian approximations to derive the distribution of capacity and discussed the implications of channel hardening for scheduling and rate feedback. The channel hardening phenomenon was observed in [22] when selecting an optimum antenna. The work in [22] was expanded to the case of multiple antenna selection in terms of energy efficiency in [23]. However, in the conventional works in [21–23], the channel hardening phenomena were studied in terms of capacity, without considering any practical signal processing techniques, such as linear precoders/receivers. In addition, in previous works [21–23], there were no comprehensive closed-form expressions of the variance of mutual information as a function of the number of antennas to scale the variance according to the number of antennas.

Consequently, in this paper, we investigate the scaling laws of scheduling gain for uplink multiuser massive MIMO systems in order to verify the feasibility of user scheduling for massive MIMO, assuming MF and ZF receivers at the BS for data demodulation. First, we derive the exact probability density function (PDF) of SINR and its moment-generating function (MGF) to obtain the first and second moments of SINR under the perfect channel state information (CSI) at the BS. Using Taylor series expansion, we obtain a closed-form expression for the approximated variance of the individual rate for a user as a function of the number of BS antennas. Then, using the Gaussianity of the sum rate for multiple users, the achievable scheduling gain is derived as a closed form. According to our analysis for the case of perfect CSI, as the number of antennas increases and tends towards infinity, the scheduling gain of the MF receiver increases and converges to a constant value, while that of the ZF receiver decreases to zero. Thereafter, our analysis is extended to the case of imperfect CSI at the BS. It is shown that when there is insufficient CSI available at the BS, the variance of the sum rate for the ZF receiver increases as the number of antennas increases, similar to the MF receiver. This is because the multiuser interference cannot be completely removed, owing to the imperfectness of the CSI. However, the scheduling gain of the ZF receiver still decreases to zero with the increasing number

of antennas when the user selection is performed based on the imperfect CSI. Thus, user scheduling for massive MIMO systems is still beneficial for the MF receiver, regardless of the imperfectness of CSI; however, the benefit of user scheduling is negligible for the ZF receiver.

The remainder of this paper is organized as follows. Section 2 presents an uplink massive MIMO system model with linear receivers. In Section 3, the scaling laws and feasibility of user scheduling according to the number of antennas are investigated under the assumption of perfect CSI at the BS and these results are extended to the case of imperfect CSI in Section 4. Section 5 presents the simulation results to verify our analyses, and Section 6 concludes the paper.

2. System Model

We consider an uplink multiuser MIMO system, where a BS equipped with M antennas serves K users with a single antenna. The $M \times 1$ received signal vector is expressed as

$$\mathbf{y} = \sqrt{p_u} \mathbf{H} \mathbf{x} + \mathbf{n}.$$

$\mathbf{H} = [\mathbf{h}_1, \dots, \mathbf{h}_K]$ is the $M \times K$ aggregated channel matrix, where the k th column $\mathbf{h}_k \sim \mathcal{CN}(\mathbf{0}, \mathbf{I}_M)$ represents the channel vector between the BS and user k . $\mathbf{x} = [x_1, \dots, x_K]^T$ is the $K \times 1$ signal vector, where x_k is the transmit symbol for user k with $\mathbb{E}\{|x_k|^2\} = 1$. $\mathbf{n} \sim \mathcal{CN}(\mathbf{0}, \mathbf{I}_M)$ is the $M \times 1$ additive white Gaussian noise vector with unit variance, and p_u is the uplink power. Using a linear receiver, the BS can obtain K streams for K users from the received signal \mathbf{y} . Let \mathbf{G} be the $M \times K$ matrix for the linear receiver. We consider two linear receivers, MF and ZF, i.e.,

$$\mathbf{G} = \begin{cases} \mathbf{H} & \text{for MF receiver} \\ \mathbf{H}(\mathbf{H}^H \mathbf{H})^{-1} & \text{for ZF receiver.} \end{cases} \quad (1)$$

Therefore, using the linear receiver, the k th stream for user k is expressed as:

$$\begin{aligned} r_k &= \mathbf{g}_k^H \mathbf{y} \\ &= \sqrt{p_u} \mathbf{g}_k^H \mathbf{h}_k x_k + \sqrt{p_u} \sum_{j \neq k} \mathbf{g}_k^H \mathbf{h}_j x_j + \mathbf{g}_k^H \mathbf{n}, \end{aligned}$$

where \mathbf{g}_k is the k th column of \mathbf{G} , which represents the receiver vector for the k th user and \mathbf{h}_j is the channel between the BS and the j th user. Therefore, the received SINR for user k is expressed as:

$$\gamma_k = \frac{p_u |\mathbf{w}_k^H \mathbf{h}_k|^2}{p_u \sum_{j \neq k} |\mathbf{w}_k^H \mathbf{h}_j|^2 + 1}, \quad (2)$$

where $\mathbf{w}_k = \mathbf{g}_k / \|\mathbf{g}_k\|$ is the normalized receive vector.

3. Scaling Laws of Scheduling Gain—Perfect CSI

In this section, we derive the scaling laws of scheduling gain for optimal user scheduling in terms of the number of BS antennas under the assumption of perfect CSI at the BS, i.e., no channel estimation errors. Thus, we obtain the variance of the individual rate and a closed-form expression for the achievable scheduling gain.

3.1. Individual Rate Analysis

According to the Shannon capacity formula [24], the individual rate for user k is defined as

$$R_k = \log_2(1 + \gamma_k). \quad (3)$$

To understand the fluctuations of the individual rate, it is necessary to analyze the second moment of mutual information. The direct derivation of the exact distribution of the mutual information

is unfeasible [25]; thus, the approximated second moment is obtained in this subsection. For (3), the Taylor series is obtained as follows:

$$\log_2(1 + \gamma_k) = \log_2 e \left(\log(1 + \mu_\gamma) + \sum_{n=1}^{\infty} \frac{(-1)^{n-1}}{n} \frac{(\gamma_k - \mu_\gamma)^n}{(1 + \mu_\gamma)^n} \right), \tag{4}$$

where $\mu_\gamma = \mathbb{E}\{\gamma_k\}$. From the definition of the joint cumulant moment of n random variables X_1, \dots, X_n [26], we can obtain

$$\begin{aligned} \kappa_n &= \mathbb{E}_c \{X_1, X_2, \dots, X_n\} \\ &\triangleq \sum_{\psi} (-1)^{|\psi|-1} (|\psi|-1)! \prod_{\beta \in \psi} \mathbb{E} \left\{ \prod_{i \in \beta} X_i \right\}, \end{aligned} \tag{5}$$

where ψ runs through all partitions of $\{1, \dots, n\}$, $|\psi|$ denotes the number of blocks in ψ , and β runs through the list of all blocks of ψ . From (4) and (5), the second cumulant moment, i.e., the variance of individual rate, can be expressed as

$$\begin{aligned} \kappa_2 &= \mathbb{E}_c \{ \log_2(1 + \gamma_k), \log_2(1 + \gamma_k) \} \\ &= (\log_2 e)^2 \sum_{m=1}^{\infty} \sum_{n=1}^{\infty} \frac{(-1)^{m+n}}{mn} \frac{\mathbb{E}_c \{ (\gamma_k - \mu_\gamma)^m, (\gamma_k - \mu_\gamma)^n \}}{(1 + \mu_\gamma)^{m+n}} \end{aligned} \tag{6}$$

$$\stackrel{(a)}{\approx} \frac{(\log_2 e)^2 \sigma_\gamma^2}{(1 + \mu_\gamma)^2}. \tag{7}$$

Here, the approximation (a) is obtained by neglecting the higher-order terms in the summation in (6), and $\sigma_\gamma^2 = \text{Var} \{ \gamma_k \}$. Therefore, as shown in (7), the moments of the SINR, μ_γ and σ_γ^2 , should be derived to obtain the variance of mutual information.

Next, the variance of the mutual information is analyzed for the case of the MF receiver. Thus, we first derive the following lemma:

Lemma 1. For a random variable $Z \triangleq \frac{aX}{bY+1}$, where $X \sim \mathcal{X}_{2d_1}^2$, $Y \sim \mathcal{X}_{2d_2}^2$, and X and Y are independent, the PDF of Z is expressed as

$$f_Z(z) = \frac{d_1 \left(\frac{z}{a}\right)^{d_1-1} e^{-\frac{z}{a}}}{a\Gamma(d_2)} \sum_{i=0}^{d_1} \frac{(i+d_2-1)! b^i}{(d_1-i)! i!} \left(\frac{b}{a}z + 1\right)^{-(i+d_2)}. \tag{8}$$

Furthermore, the MGF of Z is expressed as

$$\mathcal{M}_Z(s) = \frac{d_1 \Gamma(d_1)}{\Gamma(d_2)} \sum_{i=0}^{d_1} \frac{(i+d_2-1)! b^{i-d_1}}{(d_1-i)! i!} \times \Psi \left(d_1, 1 + d_1 - i - d_2, \frac{1}{b} - \frac{a}{b}s \right), \tag{9}$$

where $\Gamma(x) = \int_0^\infty t^{x-1} e^{-t} dt$ is the Gamma function; $\Psi(a, b, s)$ is the confluent hypergeometric function of the second kind, which is defined by $\Psi(a, b, s) = \frac{1}{\Gamma(a)} \int_0^\infty e^{-st} t^{a-1} (1+t)^{b-a-1} dt$ [27].

Proof of Lemma 1. See Appendix A. \square

Using Lemma 1, we can obtain the PDF and MGF of the SINR for the MF receiver.

Corollary 1. The PDF and MGF of the SINR for the MF receiver are obtained from Lemma 1 after substituting $d_1 = M$, $d_2 = K - 1$, and $a = b = p_u$.

Proof of Corollary 1. Let $v_j \triangleq |\mathbf{w}_k^H \mathbf{h}_j|^2 = |\mathbf{h}_k^H \mathbf{h}_j|^2 / \|\mathbf{h}_k\|^2 \forall j$. Then, the SINR for the MF receiver is expressed as

$$\gamma_{k, MF} = \frac{p_u v_k}{p_u \sum_{j \neq k} v_j + 1}.$$

v_k in the numerator of $\gamma_{k, MF}$ follows the chi-square distribution with $2M$ degrees of freedom. Furthermore, $\sum_{j \neq k} v_j$ in the denominator of $\gamma_{k, MF}$ follows the chi-square distribution with $2(K - 1)$ degrees of freedom because each $v_j \sim \text{Exp}(1)$ and the summation of independent $(K - 1)$ $\text{Exp}(1)$ random variables follow a chi-square distribution with $2(K - 1)$ degrees of freedom [28]. In [29], it was proven that v_k is independent of v_j for $\forall j \neq k$. Therefore, we can obtain the PDF and the MGF of the SINR of the MF receiver directly from Lemma 1. \square

Although the MGF in Lemma 1 is a closed-form expression, it is still a challenge to explicitly understand the dependence of the variance on the number of BS antennas M . Therefore, to obtain a simplified form of the variance, we use the following lemma:

Lemma 2. Consider two chi-square random variables $X \sim \mathcal{X}_{2d_1}^2$ and $Y \sim \mathcal{X}_{2d_2}^2$. Then a random variable $Z \triangleq \frac{d_2}{d_1} \cdot \frac{X}{Y}$ follows $\mathcal{F}(2d_1, 2d_2)$, i.e., the PDF of Z is expressed as:

$$f_Z(z; 2d_1, 2d_2) = \frac{\Gamma(d_1 + d_2)}{\Gamma(d_1) \Gamma(d_2)} \times \left(\frac{d_1}{d_2}\right)^{d_1} z^{d_1-1} \left(1 + \frac{d_1}{d_2} z\right)^{-(d_1+d_2)},$$

and the n th moment is given by:

$$\eta_n = \left(\frac{d_2}{d_1}\right)^n \frac{\Gamma(d_1 + n) \Gamma(d_2 - n)}{\Gamma(d_1) \Gamma(d_2)}. \tag{10}$$

Proof of Lemma 2. From the definition of F distributions [30], this is straightforward and thus omitted here. \square

At the high p_u regime, i.e., the interference-limited environment, the noise variance in the denominator of the SINR can be neglected. Therefore, the distribution of the SINR for the MF receiver can be approximated as a scaled F distribution, i.e., $\frac{K-1}{M} \gamma_{k, MF} \sim F(2M, 2(K - 1))$. Therefore, using (10) in Lemma 2, we obtain the first and second moments of the SINR for the MF receiver as follows:

$$\mu_\gamma = \frac{M}{K-2} \quad \text{and} \quad \sigma_\gamma^2 = \frac{M(M+K-2)}{(K-2)^2(K-3)}. \tag{11}$$

By substituting the mean and variance of the SINR of (11) into (7), the approximated variance of the individual rate for the MF receiver is expressed as

$$\kappa_{2, MF} \approx \frac{(\log_2 e)^2 M}{(M+K-2)(K-3)}. \tag{12}$$

Hereafter, the variance of mutual information is analyzed for the case of the ZF receiver. For the ZF receiver, because $|\mathbf{w}_k^H \mathbf{h}_k|^2 = 1/\|\mathbf{g}_k\|^2$ and $|\mathbf{w}_k^H \mathbf{h}_j|^2 = 0$ for $\forall j \neq k$, the SINR is obtained as

$$\gamma_{k, ZF} = p_u / \|\mathbf{g}_k\|^2.$$

Because $\gamma_{k, ZF}$ follows the chi-square distribution, with $2(M - K + 1)$ degrees of freedom [31], the first and second moments of the SINR can be represented in terms of M and K from the MGF of a chi-square distribution as follows:

$$\mu_\gamma = p_u(M - K + 1) \quad \text{and} \quad \sigma_\gamma^2 = p_u^2(M - K + 1). \tag{13}$$

By substituting (13) into (7), we can approximate the variance of the individual rate for the ZF receiver as:

$$\kappa_{2,ZF} \approx \frac{p_u^2 (\log_2 e)^2 (M - K + 1)}{(p_u (M - K + 1) + 1)^2}. \tag{14}$$

From the analysis, the following scaling laws of the individual rate with perfect CSI can be observed. For the MF receiver, the variance of the individual rate $\kappa_{2,MF}$ is a monotonically increasing function of M , which then scales with $\mathcal{O}(1)$ as $M \rightarrow \infty$. Conversely, the variance of the individual rate for the ZF receiver $\kappa_{2,ZF}$ decreases with $\mathcal{O}(\frac{1}{M})$ and converges to zero as M increases. Thus, the analysis indicates that the channel hardening effect occurs only for the ZF receiver, while the fluctuation of mutual information for the MF receiver becomes large as the number of antennas increases.

3.2. Sum Rate Analysis

The scheduling gain is related to the fluctuations in the mutual information; thus, more scheduling gain can be realized as the fluctuations in the sum rate become larger. To explicitly understand the relationship between the variance of sum rate and the scheduling gain, we introduce the result in [21] with a slight modification.

We assume that the BS selects K active users among N total users through a user scheduling algorithm. Let R denote the sum rate, that is, $R \triangleq \sum_{k=1}^K R_k$ and \mathcal{R} denote the achievable rate, defined as the maximum sum rate after the optimal multiuser scheduling, that is

$$\mathcal{R} \triangleq \max_{S \subset \{1, \dots, N\}, |S|=K} R(S),$$

where S is a set of users and $R(S) \triangleq \sum_{k \in S} R_k$. Combining the Gaussianity of the sum rate of the linear receiver [25] and the results in [21], we can approximate the achievable rate \mathcal{R} as

$$\mathcal{R} \approx \mu_R + \sqrt{2\sigma_R^2 \log \binom{N}{K}}, \tag{15}$$

where μ_R and σ_R^2 are the mean and variance of R , respectively. According to (15), the maximum scheduling gain by the optimum algorithm is approximately $\sqrt{2\sigma_R^2 \log \binom{N}{K}}$.

Hereafter, we investigate the variance of the sum rate σ_R^2 to understand the achievable scheduling gain with respect to the number of antennas. Using the results in [25], the second-order joint cumulant moment of R can be expressed as

$$\begin{aligned} \kappa_2^{sum} &= \sum_{m=1}^K \sum_{n=1}^K \mathbb{E}_c [R_m, R_n] \\ &= \sum_{m=1}^K \mathbb{E}_c [R_m, R_m] + \sum_{m=1}^K \sum_{\substack{n=1 \\ n \neq m}}^K \mathbb{E}_c [R_m, R_n] \\ &\stackrel{(a)}{=} K \mathbb{E}_c [R_1, R_1] + K(K-1) \mathbb{E}_c [R_1, R_2] \\ &\stackrel{(b)}{\approx} (\log_2 e)^2 K \frac{\sigma_\gamma^2}{(1 + \mu_\gamma)^2} + (\log_2 e)^2 K(K-1) \frac{\mathbb{E}[\gamma_1 \gamma_2] - \mu_\gamma^2}{(1 + \mu_\gamma)^2}. \end{aligned} \tag{16}$$

Here, (a) follows the symmetry of the joint cumulant matrix, [25] and (b) follows the same approximation used in (7). Although the first term of (16), the variance of the individual rate, was already derived, the second term of (16), the covariance of the SINR, should be derived and is defined as $\text{Cov}[\gamma_1, \gamma_2] = \mathbb{E}[\gamma_1 \gamma_2] - \mathbb{E}[\gamma_1] \mathbb{E}[\gamma_2]$. To calculate the exact covariance, the joint PDF of $Z \triangleq \gamma_1 \gamma_2$ is required. However, the joint PDF is intractable because γ_1 and γ_2 are not independent of each other.

Therefore, as an alternative approach for the MF receiver, we consider a lower bound of the variance of the sum rate by considering only the first term in (16). Substituting (12) into the first term

in (16), we obtain the lower bound for the variance of the sum rate for the MF receiver at the high p_u regime as follows:

$$\kappa_{2, MF}^{sum} > \frac{(\log_2 e)^2 MK}{(M + K - 2)(K - 3)}. \tag{17}$$

Meanwhile, for the ZF receiver, the approximated covariance of the SINR can be derived as $\text{Cov}[\gamma_1, \gamma_2] \approx p_u^2$ in [25] by the joint distribution of the eigenvalues and Noviokv’s theorem. By combining (14) and (16), the approximated variance of the sum rate for the ZF receiver can be obtained as

$$\kappa_{2, ZF}^{sum} \approx \frac{p_u^2 (\log_2 e)^2 MK}{(1 + p_u (M - K + 1))^2}. \tag{18}$$

From (17) and (18), it is observed that the scaling laws of the sum rate are equivalent to those of the individual rate. As M tends towards infinity, i.e., massive MIMO, the variance of the sum rate for the ZF receiver decreases to zero, while that for the MF receiver increases to a constant value. Therefore, by substituting (17) and (18) into (15), we can observe the following aspects:

- For the MF receiver, the scheduling gain first increases and then scales with $\mathcal{O}(1)$ as $M \rightarrow \infty$ under perfect CSI. This implies that the user scheduling to maximize the sum rate is still beneficial for massive MIMO systems with the MF receiver.
- For the ZF receiver, the scheduling gain decreases with $\mathcal{O}\left(\sqrt{\frac{1}{M}}\right)$ under the perfect CSI. Therefore, if the ZF receiver is used at the BS, only a limited scheduling gain can be achievable for large M . This implies that the benefit of user scheduling tends to disappear for massive MIMO systems using the ZF receiver.

4. Scaling Laws of Scheduling Gain—Imperfect CSI

In this section, we extend the scaling laws of the scheduling gain of optimal user scheduling in Section 3 to the case of imperfect CSI at the BS.

The imperfectness of CSI affects two major operations at the BS: data demodulation and user scheduling. For data demodulation, the imperfect CSI typically implies a CSI with a channel estimation error that occurs due to the use of a practical channel estimator at the BS. The channel estimation error causes additional multiuser interference; thus, the channel hardening effect for the cases of imperfect CSI will be different compared to that for the perfect CSI case. Conversely, from the user scheduling perspective, the CSI imperfectness corresponds to the degree of CSI availability for calculating proper user selection metrics to determine a set of users to be scheduled. The CSI availability for user scheduling can be affected by not only the accuracy of the estimated channel, but also the extra channel-related information, which can contribute to better user selection. Thus, we consider two scenarios of CSI availability for user scheduling: non-ideal CSI availability as the worst case and near-ideal CSI availability as the best case. Based on these scenarios, which will be explained in detail later in this section, the effect of imperfect CSI on the scaling laws of scheduling gain will be investigated.

We begin by analyzing the effect of imperfect CSI on the fluctuation of individual rate. Without loss of generality, the estimated channel $\hat{\mathbf{h}}_k$ of user k can be modeled as [18]:

$$\mathbf{h}_k = \sqrt{1 - \tau^2} \hat{\mathbf{h}}_k + \tau \mathbf{e}_k, \tag{19}$$

where $\mathbf{e}_k \sim \mathcal{CN}(\mathbf{0}, \mathbf{I}_M)$ is the Gaussian noise vector uncorrelated with $\hat{\mathbf{h}}_k$ and $\tau \in [0, 1]$, which represents the imperfectness of $\hat{\mathbf{h}}_k$. Typically, τ is determined by the pilot sequence length t_p and pilot power p_p , such as $\tau = \sqrt{\frac{1}{t_p p_p + 1}}$ when the estimated channel is obtained by the MMSE channel estimator, assuming that the orthogonal uplink pilot sequences are used across the users, as indicated

in [32]. Based on the estimated channel, the receiver matrix $\hat{\mathbf{G}}$ is calculated as (1) at the BS, and the received k th stream and corresponding received SINR for user k are expressed as:

$$\begin{aligned} r_k &= \sqrt{p_u} \hat{\mathbf{g}}_k^H \mathbf{h}_k x_k + \sqrt{p_u} \sum_{j \neq k} \hat{\mathbf{g}}_k^H \mathbf{h}_j x_j + \hat{\mathbf{g}}_k^H \mathbf{n} \\ &= \sqrt{p_u (1 - \tau^2)} \hat{\mathbf{g}}_k^H \hat{\mathbf{h}}_k x_k + \sqrt{p_u \tau^2} \hat{\mathbf{g}}_k^H \mathbf{e}_k x_k + \sqrt{p_u} \sum_{j \neq k} \hat{\mathbf{g}}_k^H \mathbf{h}_j x_j + \hat{\mathbf{g}}_k^H \mathbf{n}, \end{aligned}$$

and

$$\gamma_k^{ip} = \frac{p_u (1 - \tau^2) \left| \hat{\mathbf{w}}_k^H \hat{\mathbf{h}}_k \right|^2}{p_u \tau^2 \left| \hat{\mathbf{w}}_k^H \mathbf{e}_k \right|^2 + p_u \sum_{j \neq k} \left| \hat{\mathbf{w}}_k^H \mathbf{h}_j \right|^2 + 1}, \tag{20}$$

where $\hat{\mathbf{w}}_k = \hat{\mathbf{g}}_k / \|\hat{\mathbf{g}}_k\|$ is the normalized k th column vector of $\hat{\mathbf{G}}$.

Next, for the MF receiver, the PDF and MGF of the SINR are derived. Considering imperfect CSI, we introduce Lemma 3.

Lemma 3. For a random variable $Z \triangleq \frac{aX}{bY_1 + cY_2 + 1}$, where $X \sim \chi_{2d_1}^2$, $Y_1 \sim \chi_{2d_2}^2$, and $Y_2 \sim \text{Exp}(1)$, the PDF of Z is obtained by

$$f_Z(z) = \frac{d_1 \left(\frac{c-b}{c}\right)^{-d_2} \left(\frac{z}{a}\right)^{d_1-1} e^{-\frac{z}{a}}}{ac} \times \left(\sum_{l=0}^{d_1} \mathcal{A}_1 \left(\frac{z}{a} + \frac{1}{c}\right)^{-(l+1)} - \sum_{i=0}^{d_2-1} \sum_{p=0}^{d_1} \mathcal{A}_2 \left(\frac{z}{a} + \frac{1}{b}\right)^{-(p+i+1)} \right). \tag{21}$$

Here, $\mathcal{A}_1 = \frac{1}{(d_1-l)!}$ and $\mathcal{A}_2 = \frac{(p+i)! \left(\frac{1}{b} - \frac{1}{c}\right)^i}{(d_1-p)! p! i!}$. Moreover, the MGF of Z is obtained by

$$\begin{aligned} \mathcal{M}_Z(s) &= \frac{d_1 \left(1 - \frac{b}{c}\right)^{-d_2}}{c} \sum_{l=0}^{d_1} \mathcal{A}_1 Y \left(d_1, l, \frac{1}{c}, (1 - as)\right) \\ &\quad - \frac{d_1 \left(1 - \frac{b}{c}\right)^{-d_2}}{c} \sum_{i=0}^{d_2-1} \sum_{p=0}^{d_1} \mathcal{A}_2 Y \left(d_1, p+i, \frac{1}{b}, (1 - as)\right), \end{aligned} \tag{22}$$

where $Y(a, b, c, s)$ is defined as

$$\begin{aligned} Y(a, b, c, s) &= c^{a-b-1} \frac{\Gamma(a) \Gamma(1-a+b)}{\Gamma(1+b)} {}_1F_1(a, a-b, cs) \\ &\quad + s^{1-a+b} \Gamma(a-b-1) {}_1F_1(1+b, 2-a+b, cs), \end{aligned} \tag{23}$$

and ${}_pF_q(a, b, s)$ represents the generalized hypergeometric series [27].

Proof of Lemma 3. See Appendix B. \square

From Lemma 3, we can obtain the PDF and MGF of the SINR for the MF receiver under imperfect CSI.

Corollary 2. Under imperfect CSI, the PDF and MGF of the SINR for the MF receiver are obtained from Lemma 3 after substituting $d_1 = M$, $d_2 = K - 1$, $a = p_u(1 - \tau^2)$, $b = p_u$, and $c = p_u \tau^2$.

Proof of Corollary 2. Let $\nu_k \triangleq \left| \hat{\mathbf{w}}_k^H \hat{\mathbf{h}}_k \right|^2$, $\zeta_j \triangleq \left| \hat{\mathbf{w}}_k^H \mathbf{h}_j \right|^2 \forall j$ and $\varepsilon_k \triangleq \left| \hat{\mathbf{w}}_k^H \mathbf{e}_k \right|^2$. The SINR for the MF receiver under imperfect CSI conditions is obtained by

$$\gamma_{k, MF}^{ip} = \frac{p_u (1 - \tau^2) \nu_k}{p_u \tau^2 \varepsilon_k + p_u \sum_{j \neq k} \zeta_j + 1}.$$

As presented in the proof of Corollary 1, $v_k \sim \mathcal{X}_{2M}^2$ and $\sum_{j \neq k} \zeta_j \sim \mathcal{X}_{2(K-1)}^2$. $\varepsilon_k \sim \text{Exp}(1)$ because $\hat{\mathbf{w}}_k$ is a unit-norm random vector, independent of the Gaussian random vector \mathbf{e}_k [33]. In addition, v_k , $\sum_{j \neq k} \zeta_j$ and ε_k are independent of each other. Therefore, we obtain Corollary 2 from Lemma 3. \square

To obtain a closed-form expression for the variance of the individual rate, we again use the F approximation. In the high τ regime, the total interference term in the denominator of $\gamma_{k, MF}^{ip}$ follows an approximate chi-square distribution with $2K$ degrees of freedom, that is, $\tau^2 |\hat{\mathbf{w}}_k^H \mathbf{e}_k|^2 + \sum_{j \neq k} |\hat{\mathbf{w}}_k^H \mathbf{h}_j|^2 \sim \mathcal{X}_{2K}^2$. Therefore, the SINR of the MF receiver can be approximated as a scaled F distribution as $\left(\frac{K}{(1-\tau^2)M}\right) \gamma_{k, MF}^{ip} \sim F(2M, 2K)$ in the high p_u regime. Therefore, assuming (7) and (10), the variance of the individual rate for the MF receiver under imperfect CSI can be approximated as

$$\kappa_{2, MF}^{(ip)} \approx \frac{(\log_2 e)^2 (1 - \tau^2)^2 M (M + K - 1)}{(K - 2) (K - 1 + (1 - \tau^2) M)^2}. \tag{24}$$

Meanwhile, for the ZF receiver, the PDF and MGF of the SINR under the imperfect CSI can be obtained from Lemma 1.

Corollary 3. Under imperfect CSI, the PDF and MGF of the SINR for the ZF receiver are obtained from Lemma 1 after substituting $d_1 = M - K + 1$, $d_2 = K$, $a = p_u(1 - \tau^2)$ and $b = p_u \tau^2$.

Proof of Corollary 3. Let $v_k \triangleq |\hat{\mathbf{w}}_k^H \hat{\mathbf{h}}_k|^2$ and $\varepsilon_j \triangleq |\hat{\mathbf{w}}_k^H \mathbf{e}_j|^2 \forall j$. Then, the SINR for the ZF receiver under imperfect CSI is given by

$$\gamma_{k, ZF}^{ip} = \frac{p_u (1 - \tau^2) v_k}{p_u \tau^2 \sum_j \varepsilon_j + 1}$$

because $\hat{\mathbf{w}}_k^H \hat{\mathbf{h}}_j = 0$ for $\forall j \neq k$. $v_k \sim \mathcal{X}_{2(M-K+1)}^2$ and $\sum_j \varepsilon_j \sim \mathcal{X}_{2K}^2$. Moreover, v_k and $\sum_j \varepsilon_j$ are independent of each other [33]. Therefore, we obtain Corollary 3 from Lemma 1. \square

Similar to the case of the MF receiver, the SINR of the ZF receiver in the high p_u regime can be approximated as a scaled F distribution as $\left(\left(\frac{\tau^2}{1-\tau^2}\right) \frac{K}{M-K+1}\right) \gamma_{k, ZF}^{ip} \sim F(2(M - K + 1), 2K)$. Therefore, using (7) and (10), the variance of the individual rate for the ZF receiver under imperfect CSI is expressed as

$$\kappa_{2, ZF}^{(ip)} \approx \frac{(\log_2 e)^2 (1 - \tau^2)^2 (M - K + 1) M}{(\tau^2 (K - 1) + (1 - \tau^2) (M - K + 1))^2 (K - 2)}. \tag{25}$$

From the analysis, the following scaling laws of the individual rate with imperfect CSI can be observed. For the MF receiver, the variance of the individual rate $\kappa_{2, MF}^{(ip)}$ is a monotonically increasing function of M (Appendix C) and scales with $\mathcal{O}(1)$ as $M \rightarrow \infty$. That is, the fluctuation characteristic of the individual rate for the MF receiver does not change according to the imperfectness of CSI. However, the channel hardening of the ZF receiver depends on τ (Appendix D). As M increases, the variance of the individual rate $\kappa_{2, ZF}^{(ip)}$ tends to monotonically increase for a large τ , whereas $\kappa_{2, ZF}^{(ip)}$ tends to decrease monotonically for a small τ . Thus, $\kappa_{2, ZF}^{(ip)}$ is scaled with $\mathcal{O}(1)$ as $M \rightarrow \infty$ for a large τ , and the channel hardening effect for the ZF receiver occurs only in the low τ regime. This is because the multiuser interference for the ZF receiver increases with τ .

Hereafter, the scaling laws of the scheduling gain under imperfect CSI are investigated. We first consider the case in which the user scheduling relies on non-ideal CSI availability, assuming that the estimated channel is directly used for the user selection algorithm, as in [13,17]. In this scenario, the BS will regard the estimated channel as the actual channel as the BS cannot estimate the channel estimation error by itself. Thus, a metric for user selection can be calculated by the estimated channel, and the BS can select several users to be served based on the calculated metrics. Accordingly, it can

be observed from (15) that the achievable scheduling gain follows $\sqrt{2\sigma_{\hat{R}}^2 \log \binom{N}{K}}$, where $\hat{R} = \sum_k \hat{R}_k$ corresponds to the estimated sum rate derived from the estimated SINR in (2), after replacing \mathbf{h} with $\hat{\mathbf{h}}$. Therefore, we can expect that there is no difference between the scaling laws of scheduling gain with imperfect and perfect CSI.

Next, we determine the scaling laws when the near-ideal CSI is available for user scheduling. As mentioned earlier, there can be extra channel-related information available on top of the estimated channel at the BS, for user scheduling purposes. A typical example of obtaining additional information is to use sounding reference signals, as specified in 5G NR [34]; the additional uplink pilot used for SINR estimation, channel quality estimation, and beam direction estimation improves the user scheduling and is not directly related to uplink data demodulation. For simplicity, we assume that the exact SINR in (20) is available at the BS and used for the user selection metric in the case of near-ideal CSI availability. Then, it is observed from (15) that the achievable scheduling gain under near-ideal CSI availability can be obtained by $\sqrt{2\sigma_{\tilde{R}}^2 \log \binom{N}{K}}$, where \tilde{R} is derived from the exact SINR in (20). In this case, two different SINRs γ_1 and γ_2 in (16) are not independent of each other, even for the ZF receiver, because, unlike perfect CSI, there is residual multiuser interference under imperfect CSI. For tractable analysis, we consider the lower bounds for the variance of the sum rate for both MF and ZF receivers. By substituting (24) and (25) into the first term in (16), we obtain

$$\kappa_{2,MF}^{sum,(ip)} > \frac{(\log_2 e)^2 (1 - \tau^2)^2 M (M + K - 1) K}{(K - 2) (K - 1 + (1 - \tau^2) M)^2} \quad (26)$$

and

$$\kappa_{2,ZF}^{sum,(ip)} > \frac{(\log_2 e)^2 (1 - \tau^2)^2 (M - K + 1) M K}{(\tau^2 (K - 1) + (1 - \tau^2) (M - K + 1))^2 (K - 2)}. \quad (27)$$

From (26) and (27), it is observed that the scaling law for the variance of the sum rate is the same as that of the individual rate.

Finally, we can summarize the scaling laws of the scheduling gain with imperfect CSI as follows:

- If non-ideal CSI is available for user scheduling at the BS, the scaling law of the scheduling gain with imperfect CSI is similar to that with perfect CSI. That is, under imperfect CSI for data demodulation with non-ideal CSI for user scheduling, the user selection is still beneficial for the MF receiver, whereas this benefit is negligible for the ZF receiver.
- If near-ideal CSI is available for user scheduling at the BS, i.e., under imperfect CSI for data demodulation with near-ideal CSI for user scheduling, the scaling law of the scheduling gain for the MF receiver with imperfect CSI is similar to that with perfect CSI. However, the scaling law of the scheduling gain for the ZF receiver under imperfect CSI is different from that under perfect CSI and depends on the channel estimation error τ . In the low τ regime, the scheduling gain decreases. Meanwhile, in the high τ regime, the scheduling increases as M increases and eventually converges to a constant value, i.e., scaled by $\mathcal{O}(1)$ as $M \rightarrow \infty$. Therefore, under imperfect CSI for data demodulation, with near-ideal CSI for user scheduling, the user selection is still beneficial for the MF receiver, whereas it can be different for the ZF receiver depending on the imperfectness of CSI.

5. Simulation Results

In this section, simulation results are provided to verify our analyses. First, in Figure 1, the analytical PDFs of the SINR in the corollaries are compared with the simulation results, where $M = 64$, $K = 20$, $p_u = 20$ dB, and $\tau^2 = 0.2$. The symbols represent the simulation results, and the lines depict the analytical results. From Figure 1, the derived PDFs match well with the simulation results.

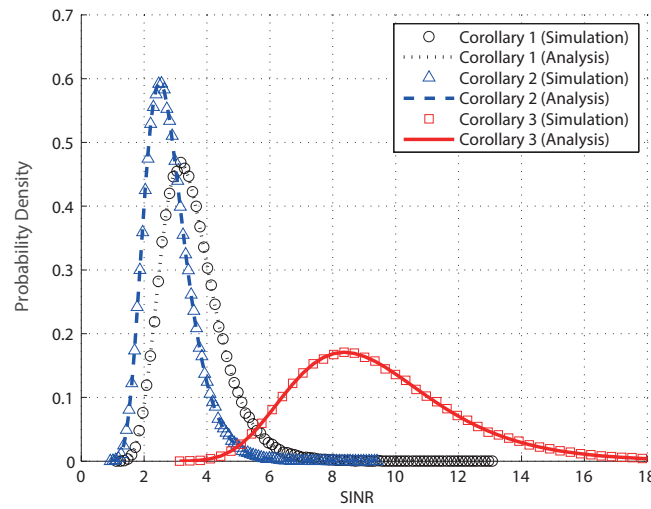


Figure 1. Comparison between the Monte Carlo simulations and analytical probability density functions (PDFs) of signal-to-interference-plus-noise ratio (SINR), where $M = 64$, $K = 20$, $p_u = 20$ dB, and $\tau^2 = 0.2$.

From Figure 2–9, simulation results for the ergodic sum rates and scheduling gains of user selection algorithms as well as the variances of individual rates and sum rates are shown. The margin of error considering the 95% confidence interval for each point is about $2.73 \cdot 10^{-2}$ at maximum.

Figure 2 shows the variances of individual rate under perfect CSI according to M when $K = 20$ and $p_u = 20$ dB. For the MF receiver, two analytical results are considered: (7) after substituting the exact μ_γ and σ_γ^2 obtained by the MGF in Corollary 1, and (12) obtained by the F approximation. For the ZF receiver, the analytical result corresponds to (14). For the MF receiver, it is observed that the analytical results with the exact moments and F approximation are almost the same. The difference between the simulation and analytical results is due to neglecting the higher-order moments of SINR in the Taylor series expansion. Therefore, we can confirm that the variance of the MF receiver increases while that of the ZF receiver decreases as M increases. That is, under perfect CSI, the MF receiver does not exhibit the channel hardening phenomenon unlike the ZF receiver, as predicted.

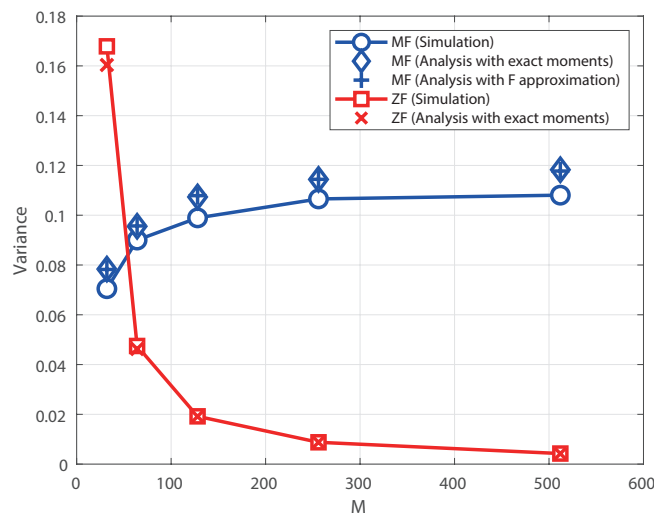


Figure 2. Variance of individual rate under perfect channel state information (CSI) as a function of M , where $K = 20$ and $p_u = 20$ dB.

Figure 3 shows the variances of the sum rate under perfect CSI as a function of M when $K = 20$ and $p_u = 20$ dB. For the MF receiver, the lower bound in (17) is represented; for the ZF receiver, the approximation in (18) is represented. Similar to the case of individual rate, the variance of the MF receiver increases, while that of the ZF receiver decreases as M increases. As demonstrated by the analysis, the sum rate of the ZF receiver still exhibits the channel hardening effect.

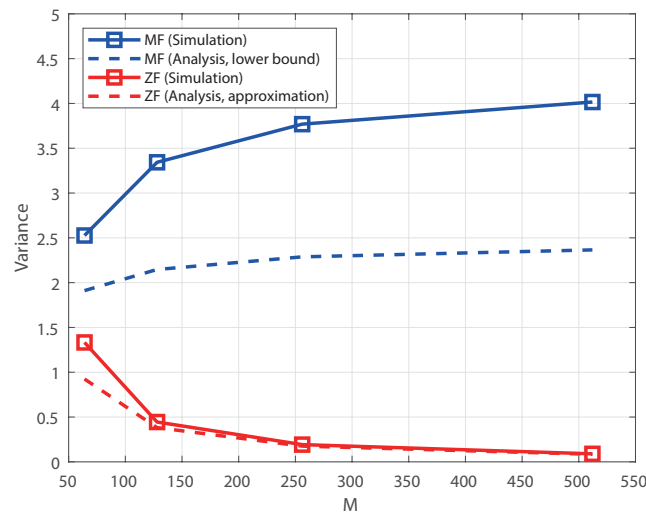


Figure 3. Variance of sum rate under perfect CSI as a function of M , where $K = 20$ and $p_u = 20$ dB.

Figure 4 illustrates the ergodic sum rate as a function of M according to the user selection algorithm at the BS under the assumption of perfect CSI, where $N = 100$, $K = 20$, and $p_u = 0$ dB. For the MF receiver, we consider SIRUS [14], which is proposed for MF-based massive MIMO systems. In SIRUS, a user who generates the maximum SIR among the remaining users is sequentially selected in a greedy manner until the number of selected users becomes equal to K . For the ZF receiver, we consider SUS [13], which is designed for the ZF to maximize the sum rate. In SUS, a user set with near-orthogonal channel vectors is selected in the greedy manner. For comparison, the results of round robin (RR) scheduling and the achievable maximum sum rate in (15), i.e., optimal user scheduling, are presented. The RR scheduler selects the users randomly; hence, no scheduling gain occurs. Meanwhile, the maximum sum rate in (15) can be realized when an optimal user selection algorithm based on an exhaustive search is employed. Therefore, the simulation of the computational complexity of the optimal scheduler is infeasible; thus, the analytical results of (15) are shown, rather than the simulation results. In addition to the ergodic sum rate shown in Figure 4, we plot the corresponding scheduling gain as a function of M under perfect CSI in Figure 5, where the simulation environment is equivalent to that in Figure 4. In Figure 5, the scheduling gain is defined as the performance gain of a specific user selection algorithm compared to RR in terms of the ergodic sum rate.

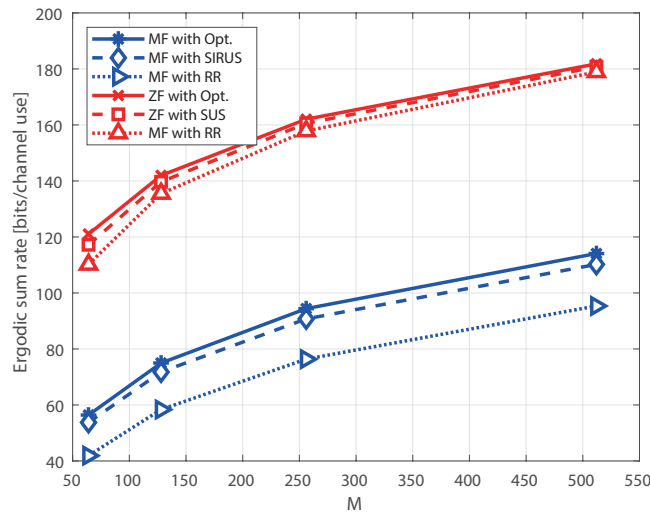


Figure 4. Ergodic sum rate under perfect CSI as a function of M , where $N = 100$, $K = 20$, and $p_u = 0$ dB.

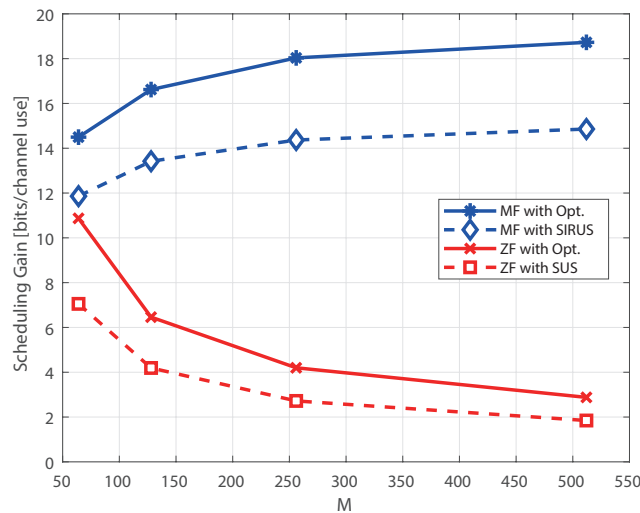


Figure 5. Scheduling gain under perfect CSI as a function of M , where $N = 100$, $K = 20$, and $p_u = 0$ dB.

As shown in Figures 4 and 5, the performance gap between the SUS and RR of the ZF receiver decreases as M increases. This is because the variance of the sum rate decreases for the ZF receiver for a large M . For the MF receiver, the gain of SIRUS increases and maintains a constant positive performance gap compared to the RR scheduler as M increases. However, the performance gap between the SUS and RR of the MF receiver shrinks as M increases, although the variance of the MF receiver increases. That is, for massive MIMO systems with SUS for the MF receiver, multiuser diversity gain is not sufficiently obtained compared to SIRUS. This implies that the user scheduling algorithm should be carefully chosen according to the types of receivers to fully utilize the multiuser diversity. From the simulation results, we can conclude that user scheduling is more important for the MF receiver than for the ZF receiver in massive MIMO systems under perfect CSI, as analyzed in Section 3.

Hereafter, the simulation results under imperfect CSI are presented from Figure 6–9. In Figure 6, the variance of the individual rate under imperfect CSI is presented as a function of M , where $N = 100$, $K = 20$, and $p_u = 0$ dB. For simplicity, the analytical results of the F approximation are omitted in Figure 6. As demonstrated by the analysis for the MF receiver, the variance of the individual rate always increases, regardless of τ . However, for the ZF receiver, the variance of the individual rate

decreases when $\tau^2 = 0.1$ and increases when $\tau^2 = 0.4$, according to M . Therefore, it can be observed from Figure 6 that the imperfectness of CSI affects the channel hardening effect for the ZF receiver. Furthermore, under imperfect CSI, all variances of the individual rate converge to a constant value as M increases.

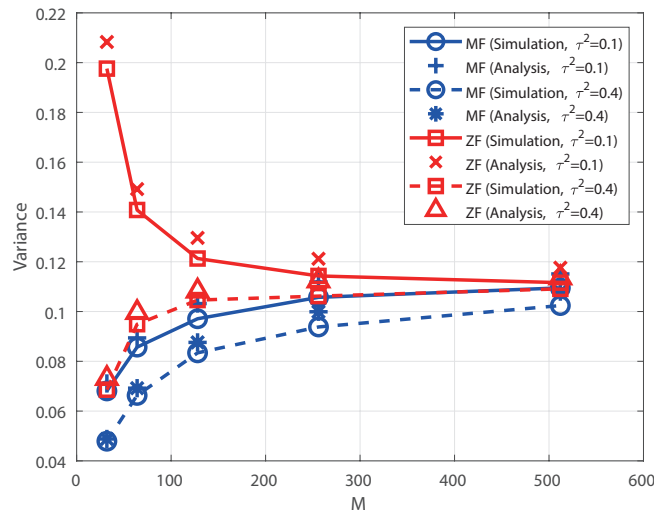


Figure 6. Variance of individual rate under imperfect CSI as a function of M , where $N = 100$, $K = 20$, and $p_u = 20$ dB.

Figure 7 shows the variance of the sum rate under imperfect CSI as a function of M , where $N = 100$, $K = 20$, and $p_u = 0$ dB. For the analytical results, the lower bounds (26) and (27) are shown for the MF and ZF receivers, respectively. Similar to the results in Figure 6, the scaling law on the variance of the sum rate with M for the MF receiver does not change, regardless of τ , while that for the ZF receiver tends to change depending on τ .

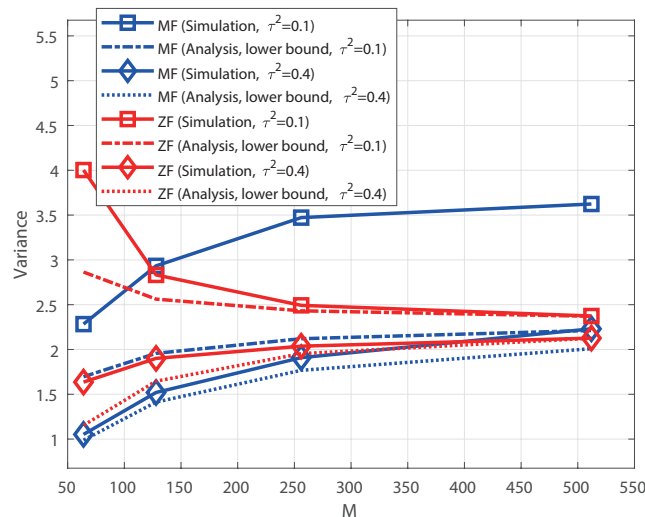


Figure 7. Variance of sum rate under imperfect CSI as a function of M , where $N = 100$, $K = 20$, and $p_u = 20$ dB.

Figure 8 represents the ergodic sum rate as a function of M with the user selection algorithm at the BS, where $N = 100$, $K = 20$, $p_u = 0$ dB and $\tau = 0.4$. Figure 9 depicts the corresponding scheduling gain. The cases of a small τ are not presented for simplicity. As explained in Section 4, we consider two scenarios for CSI availability for user scheduling at the BS, namely non-ideal CSI and near-ideal

CSI. The exhaustive search for the optimal user selection algorithm uses the exact SINR formula in (4) as the selection metric; thus, the CSI availability for user scheduling only affects the scheduling gain for the optimal user selection algorithm. Conversely, SUS and SIRUS are not influenced by the CSI availability for user scheduling because the user selection metrics are calculated using the estimated channel. Moreover, the RR scheduler is not affected by the CSI availability for user scheduling because of the random user selection.

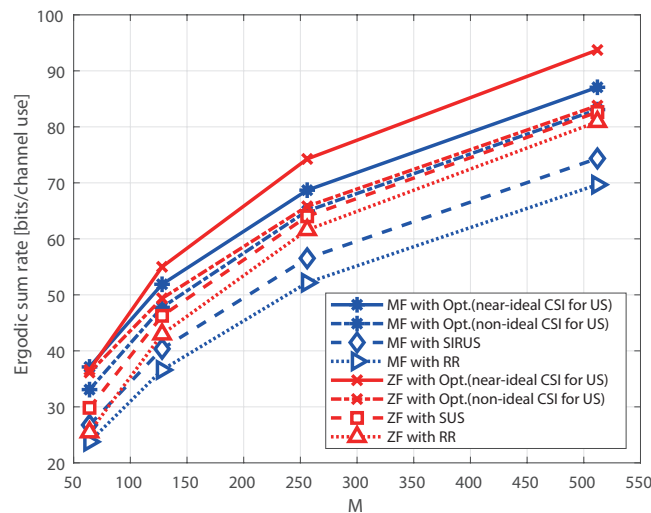


Figure 8. Ergodic sum rate under imperfect CSI as a function of M , where $N = 100$, $K = 20$, $p_u = 0$ dB, and $\tau^2 = 0.4$.

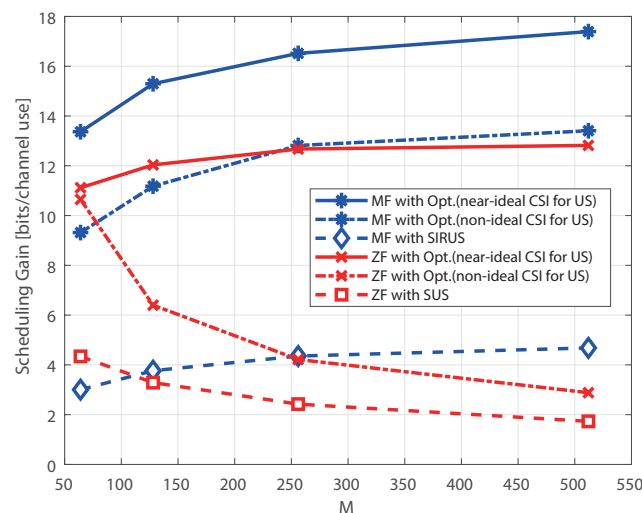


Figure 9. Scheduling gain under imperfect CSI as a function of M , where $N = 100$, $K = 20$ and $p_u = 0$ dB, and $\tau^2 = 0.4$.

From Figures 8 and 9, it is observed that the scheduling gain for the MF receiver increases as M increases, regardless of both the user selection algorithm and CSI availability for user scheduling. Simply, the scaling law for the MF receiver does not change depending on the user selection algorithm and CSI availability for user scheduling. However, the scheduling gain for the ZF receiver shows different scaling laws with M depending on the two factors. For the ZF receiver, it is observed that the scheduling gains for (i) optimal scheduler with non-ideal CSI for user scheduling and (ii) SUS decrease as M increases, while that for an optimal scheduler with near-ideal CSI for user scheduling increases with M . This implies that if near-ideal CSI is available for user scheduling, full multi-user diversity

gain from the fluctuation of the sum rate can be achieved under the optimal user selection algorithm for the ZF receiver. However, if non-ideal CSI is available for user scheduling, the achievable scheduling gain is limited, even if the optimal user selection algorithm is employed. If a typical low-complexity user selection algorithm, such as SUS, is employed, the scheduling gain for the ZF receiver decreases as M increases, even though the variance of the sum rate increases with M . Therefore, for a large τ , the benefit of user scheduling for the ZF receiver disappears under imperfect CSI provided that the user scheduling is far from optimal, and only non-ideal CSI is available for user scheduling, as analyzed in Section 4.

6. Conclusions

In this paper, we investigated the scaling laws of scheduling gain for uplink massive MIMO systems with a linear receiver. From the analyses and simulation results, we verified that the scheduling gain for the MF receiver increases as the number of antennas increases, regardless of the user selection algorithm and CSI availability for user scheduling. Furthermore, we verified that the scheduling gain for a ZF receiver can be increased only when optimal user selection is employed, under the assumption of a large channel estimation error for data demodulation and near-ideal CSI for user selection. However, optimal user selection is not practically feasible because of the enormous computational complexity of the exhaustive search. Therefore, we can conclude that random user selection is sufficient for the ZF receiver and user scheduling is still beneficial for the MF receiver in uplink massive MIMO systems. This study can be extended to more generalized massive MIMO systems with multi-antenna users and multi-cell environments under pilot contamination, as well as to state-of-the-art massive MIMO systems, such as the mmWave scenario with hybrid beamforming and large intelligent surfaces.

Author Contributions: Conceptualization, T.K. and S.P.; methodology, T.K.; software, T.K.; validation, T.K. and S.P.; formal analysis, T.K.; investigation, T.K. and S.P.; visualization, T.K.; writing—original draft preparation, T.K.; writing—review and editing, S.P.; funding acquisition, S.P. All authors have read and agreed to the published version of the manuscript.

Funding: This research was supported by the Ministry of Science and ICT (No. NRF-2019R1C1C1003202).

Conflicts of Interest: The authors declare no conflict of interest.

Appendix A. Proof of Lemma 1

For a random variable $Z \triangleq \frac{aX}{bY+1}$ with independent $X \sim \chi_{2d_1}^2$ and $Y \sim \chi_{2d_2}^2$, the PDF of Z is derived as

$$\begin{aligned}
 f_Z(z) &= \int_0^\infty f_{Z|Y}(z|y)f_Y(y) dy \\
 &= \int_0^\infty \left(\frac{by+1}{a}\right) \frac{\left(\left(\frac{by+1}{a}\right)z\right)^{d_1-1} e^{-\left(\frac{by+1}{a}\right)z}}{\Gamma(d_1)} \cdot \frac{y^{d_2-1}e^{-y}}{\Gamma(d_2)} dy \\
 &= \frac{\left(\frac{z}{a}\right)^{d_1-1} e^{-\frac{z}{a}}}{a\Gamma(d_1)\Gamma(d_2)} \int_0^\infty (by+1)^{d_1} y^{d_2-1} e^{-\left(\frac{b}{a}z+1\right)y} dy \\
 &\stackrel{(a)}{=} \frac{\left(\frac{z}{a}\right)^{d_1-1} e^{-\frac{z}{a}}}{a\Gamma(d_1)\Gamma(d_2)} \int_0^\infty \sum_{i=0}^{d_1} \binom{d_1}{i} (by)^i y^{d_2-1} e^{-\left(\frac{b}{a}z+1\right)y} dy \\
 &\stackrel{(b)}{=} \frac{d_1\left(\frac{z}{a}\right)^{d_1-1} e^{-\frac{z}{a}}}{a\Gamma(d_2)} \sum_{i=0}^{d_1} \frac{(i+d_2-1)!b^i}{(d_1-i)!i!} \left(\frac{b}{a}z+1\right)^{-(i+d_2)}, \tag{A1}
 \end{aligned}$$

where (a) follows the binomial expansion of $(by+1)^i$, and (b) comes from the equality $\int_0^\infty y^M e^{-ay} dy = M!\alpha^{-(M+1)}$. The MGF of Z in (7) is straightforwardly derived from the definition of MGF $\mathcal{M}_Z(s) = \int_0^\infty e^{sz} f_Z(z) dz$ and $\Psi(a,b,s) = \frac{1}{\Gamma(a)} \int_0^\infty e^{-st} t^{a-1} (1+t)^{b-a-1} dt$ [27].

Appendix B. Proof of Lemma 3

Let $Z \triangleq \frac{aX}{Y+1}$ and $Y \triangleq bY_1 + cY_2$, where $X \sim \mathcal{X}_{2d_1}^2$, $Y_1 \sim \mathcal{X}_{2d_2}^2$, and $Y_2 \sim \text{Exp}(1)$. First, the PDF of Y is derived as

$$\begin{aligned}
 f_Y(y) &= \int_0^\infty f_{Y|Y_1}(y|y_1) f_{Y_1}(y_1) dy_1 \\
 &= \int_0^{y/b} \frac{1}{c} e^{-\left(\frac{y-by_1}{c}\right)} \frac{y_1^{d_2-1} e^{-y_1}}{\Gamma(d_2)} dy_1 \\
 &= \frac{e^{-\frac{y}{c}}}{c\Gamma(d_2)} \int_0^{y/b} y_1^{d_2-1} e^{-\left(1-\frac{b}{c}\right)y_1} dy_1 \\
 &\stackrel{(a)}{=} \frac{e^{-\frac{y}{c}}}{c\Gamma(d_2)} \left(1-\frac{b}{c}\right)^{-d_2} \gamma\left(d_2, \left(\frac{1}{b}-\frac{1}{c}\right)y\right) \\
 &\stackrel{(b)}{=} \frac{e^{-\frac{y}{c}}}{c} \left(1-\frac{b}{c}\right)^{-d_2} \left(1 - e^{-\left(\frac{1}{b}-\frac{1}{c}\right)y} \sum_{i=0}^{d_2-1} \frac{\left(\frac{1}{b}-\frac{1}{c}\right)^i y^i}{i!}\right), \tag{A2}
 \end{aligned}$$

where (a) follows the equality $\int_0^z y^{d-1} e^{-ay} dy = \alpha^{-d} \gamma(d, \alpha z)$ and (b) comes from the relationship between the lower and upper incomplete gamma functions $\gamma(d, x) = \Gamma(d) - \Gamma(d, x)$. Then, from the PDF of Y , the PDF of Z is expressed as

$$\begin{aligned}
 f_Z(z) &= \int_0^\infty f_{Z|Y}(z|y) f_Y(y) dy \\
 &= \frac{\left(1-\frac{b}{c}\right)^{-d_2} \left(\frac{z}{a}\right)^{d_1-1} e^{-\frac{z}{a}}}{ac\Gamma(d_1)} \int_0^\infty (y+1)^{d_1} e^{-\left(\frac{z}{a}+\frac{1}{c}\right)y} \\
 &\quad \times \left(1 - e^{-Ay} \sum_{i=0}^{d_2-1} \frac{\left(\frac{1}{b}-\frac{1}{c}\right)^i y^i}{i!}\right) dy. \tag{A3}
 \end{aligned}$$

Meanwhile, we have

$$\int_0^\infty (y+1)^{d_1} e^{-\left(\frac{z}{a}+\frac{1}{c}\right)y} dy = \sum_{l=0}^{d_1} \frac{d_1!}{(d_1-l)!} \left(\frac{z}{a} + \frac{1}{c}\right)^{-(l+1)} \tag{A4}$$

and

$$\begin{aligned}
 &\int_0^\infty (y+1)^{d_1} e^{-\left(\frac{z}{a}+\frac{1}{c}\right)y} \left(e^{-Ay} \sum_{i=0}^{d_2-1} \frac{A^i y^i}{i!}\right) dy \\
 &= \sum_{i=0}^{d_2-1} \sum_{p=0}^{d_1} \frac{d_1! (p+i)! A^i}{(d_1-p)! p! i!} \left(\frac{z}{a} + \frac{1}{c} + A\right)^{-(p+i+1)}. \tag{A5}
 \end{aligned}$$

Therefore, by substituting (A4) and (A5) into (A3), (22) is obtained. Further, the MGF of (22) is straightforwardly obtained in the same way as Lemma 1 in Appendix A.

Appendix C. Proof of Monotonicity of (24)

Let $a \triangleq 1 - \tau^2$ and $c \triangleq K - 1$ for simplicity. Then, the first-order derivative of (24) can be written as

$$\frac{\partial \kappa_{2, MF}^{ip}}{\partial M} = \left(\frac{(\log_2 e)^2 a^2 c}{K-2}\right) \left(\frac{((2a-a^2)M^2 + 2cM + c^2)}{(aM+c)^4}\right). \tag{A6}$$

Consider the denominator of (A6), i.e., $f(M) = (2a - a^2)M^2 + 2cM + c^2$. Because $2a - a^2 \geq 0$, $f(M)$ is a convex function. Thus, the two roots of $f(M)$ are given by

$$\omega = \frac{-c \pm c\sqrt{1-a(2-a)}}{2a-a^2}. \quad (\text{A7})$$

Because $0 \leq a \leq 1$ and $c > 0$, both roots are always negative. Therefore, $f(M)$ is always positive for $M \geq K > 0$, and (24) is a monotonically increasing function of M .

Appendix D. Proof of Monotonicity of (25)

Let $a \triangleq \frac{1-\tau^2}{\tau^2}$ and $c \triangleq K-1$ for simplicity, where $a \geq 0$ and $0 < c < K$. Then, the first-order derivative of (25) is given by

$$\frac{\partial \kappa_{2,ZF}^{ip}}{\partial M} = \frac{(\log_2 e)^2 a^2 c}{(K-2)} \times \left(\frac{a(2-a)M^2 + 2c(a-1)^2 M - c^2(a-1)^2}{(a(M-c) + c)^4} \right).$$

Let $f(M) = a(2-a)M^2 + 2c(a-1)^2 M - c^2(a-1)^2$. Then, we can consider the following three cases:

- Case (i) When $a = 2$, $f(M) = 2cM - c^2$ is an increasing function of M . Since the root of $f(M)$ is $\omega = \frac{c}{2} = \frac{K-1}{2}$, $f(M)$ is always positive where $M \geq K$.
- Case (ii) When $0 \leq a < 2$, $f(M)$ is a convex function and the two roots are given by

$$\omega_1 = \frac{c(a-1)}{a} \quad \text{and} \quad \omega_2 = \frac{c(a-1)}{a-2}.$$

When $1 \leq a < 2$, $\omega_1 \geq \omega_2$ and $K > \omega_1$. When $0 \leq a < 1$, $\omega_2 > \omega_1$ and $K > \omega_2$. Therefore, $f(M)$ is always positive where $M \geq K$.

- Case (iii) When $a > 2$, $f(M)$ is a concave function and $\omega_2 > \omega_1$ and $K > \omega_2$. Therefore, $f(M)$ is always negative where $M \geq K$,

As a result, (25) is a monotonically increasing function when $0 \leq a \leq 2$, i.e., $\frac{1}{3} \leq \tau^2 \leq 1$ and (25) is a monotonically decreasing function when $a > 2$, i.e., $0 < \tau^2 < \frac{1}{3}$.

References

1. Kim, Y.; Kim, Y.; Oh, J.; Ji, H.; Yeo, J.; Choi, S.; Ryu, H.; Noh, H.; Kim, T.; Sun, F.; et al. New Radio (NR) and its Evolution toward 5G-Advanced. *IEEE Wirel. Commun.* **2019**, *3*, 2–7. [[CrossRef](#)]
2. Guevara, L.; Cheein, F.A. The Role of 5G Technologies: Challenges in Smart Cities and Intelligent Transportation Systems. *Sustainability* **2020**, *12*, 6469. [[CrossRef](#)]
3. Yeo, J.; Kim, T.; Oh, J.; Park, S.; Kim, Y.; Lee, J. Advanced Data Transmission Framework for 5G Wireless Communications in the 3GPP New Radio Standard. *IEEE Commun. Stand. Mag.* **2019**, *3*, 38–43. [[CrossRef](#)]
4. Chataut, R.; Akl, R. Massive MIMO Systems for 5G and Beyond Networks—Overview, Recent Trends, Challenges, and Future Research Direction. *Sensors* **2020**, *20*, 2753. [[CrossRef](#)] [[PubMed](#)]
5. Larsson, E.; Tufvesson, F.; Edfors, O.; Marzetta, T. Massive MIMO for Next Generation Wireless Systems. *IEEE Commun. Mag.* **2014**, *2*, 186–195. [[CrossRef](#)]
6. Rusek, F.; Persson, D.; Lau, B.K.; Larsson, E.G.; Marzetta, T.L.; Edfors, O.; Tufvesson, F. Scaling up MIMO: Opportunities and Challenges with Very Large Arrays. *IEEE Signal Process. Mag.* **2013**, *1*, 40–46. [[CrossRef](#)]
7. Marzetta, T.L. Noncooperative Cellular Wireless with Unlimited Numbers of Base Station Antennas. *IEEE Trans. Wirel. Commun.* **2010**, *11*, 3590–3600. [[CrossRef](#)]
8. Ngo, H.Q.; Larsson, E.G.; Marzetta, T.L. Energy and Spectral Efficiency of Very Large Multiuser MIMO Systems. *IEEE Trans. Commun.* **2013**, *4*, 1436–1449.

9. Lu, L.; Li, G.Y.; Swindlehurst, A.L.; Ashikhmin, A.; Zhang, R. An Overview of Massive MIMO: Benefits and Challenges. *IEEE J. Sel. Top. Signal Process.* **2014**, *5*, 742–758. [[CrossRef](#)]
10. Onggosanusi, E.; Rahman, M.S.; Guo, L.; Kwak, Y.; Noh, H.; Kim, Y.; Faxer, S.; Harrison, M.; Frenne, M.; Grant, S.; et al. Modular and High-Resolution Channel State Information and Beam Management for 5G New Radio. *IEEE Commun. Mag.* **2018**, *3*, 48–55. [[CrossRef](#)]
11. Alemaishat, S.; Saraereh, O.A.; Khan, I.; Affes, S.H.; Li, X.; Lee, J.W. An Efficient Precoding Scheme for Millimeter-Wave Massive MIMO Systems. *Electronics* **2019**, *8*, 927. [[CrossRef](#)]
12. Sharif, M.; Hassibi, B. On the Capacity of MIMO Broadcast Channels with Partial Side Information. *IEEE Trans. Inf. Theory* **2005**, *2*, 506–522. [[CrossRef](#)]
13. Yoo, T.; Goldsmith, A. On the Optimality of Multiantenna Broadcast Scheduling Using Zero-Forcing Beamforming. *IEEE J. Sel. Areas Commun.* **2006**, *3*, 528–541.
14. Kim, T.; Jung, M.; Min, K.; Kim, Y.; Lee, J.; Choi, S. Low Complexity User Scheduling Algorithm for MRT Based Massive MIMO Systems. In Proceedings of the International Conference on Electronics, Information, and Communications (ICEIC 2013), Bali, Indonesia, 30 January–2 February 2013; pp. 607–608.
15. Meng, X.; Chang, Y.; Wang, Y.; Wu, J. Multi-user Grouping Based Scheduling Algorithm in Massive MIMO Uplink Networks. In Proceedings of the 2018 IEEE 4th International Conference on Computer and Communications (ICCC), Chengdu, China, 7–10 December 2018; pp. 409–413.
16. Jiang, Z.; Chen, S.; Zhou, S.; Niu, Z. Joint User Scheduling and Beam Selection Optimization for Beam-Based Massive MIMO Downlinks. *IEEE Trans. Wirel. Commun.* **2018**, *17*, 2190–2204. [[CrossRef](#)]
17. Interdonato, G.; Karlsson, M.; Björnson, E.; Larsson, E.G. Local Partial Zero-Forcing Precoding for Cell-Free Massive MIMO. *IEEE Trans. Wirel. Commun.* **2020**, *7*, 4758–4774. [[CrossRef](#)]
18. Wagner, S.; Couillet, R.; Debbah, M.; Slock, D.T.M. Large System Analysis of Linear Precoding in Correlated MISO Broadcast Channels with Limited Feedback. *IEEE Trans. Inf. Theory* **2012**, *7*, 4509–4537. [[CrossRef](#)]
19. Hoydis, J.; Ten Brink, S.; Debbah, M. Massive MIMO in the UL/DL of Cellular Networks: How Many Antennas Do We Need? *IEEE J. Sel. Areas Commun.* **2013**, *2*, 160–171. [[CrossRef](#)]
20. Truong, K.T.; Heath, R.W., Jr. Effects of Channel Aging in Massive MIMO Systems. *J. Commun. Netw.* **2014**, *4*, 338–351. [[CrossRef](#)]
21. Hochwald, B.; Marzetta, T.; Tarokh, V. Multiple-Antenna Channel Hardening and Its Implications for Rate Feedback and Scheduling. *IEEE Trans. Inf. Theory* **2004**, *9*, 1893–1909. [[CrossRef](#)]
22. Bai, D.; Mitran, P.; Ghassemzadeh, S.S.; Miller, R.R.; Tarokh, V. Rate of Channel Hardening of Antenna Selection Diversity Schemes and Its Implication on Scheduling. *IEEE Trans. Inf. Theory* **2009**, *10*, 4353–4365. [[CrossRef](#)]
23. Li, H.; Song, L.; Debbah, M. Energy Efficiency of Large-Scale Multiple Antenna Systems with Transmit Antenna Selection. *IEEE Trans. Commun.* **2014**, *2*, 638–647. [[CrossRef](#)]
24. Cover, T.M.; Thomas, J.A. *Elements of Information Theory*; Wiley: New York, NY, USA, 1991.
25. Kumar, K.R.; Caire, G.; Moustakas, A.L. Asymptotic Performance of Linear Receivers in MIMO Fading Channels. *IEEE Trans. Inf. Theory* **2009**, *10*, 4398–4418. [[CrossRef](#)]
26. Mendel, J.M. Tutorial on Higher-Order Statistics (Spectra) in Signal Processing and Systems Theory: Theoretical Results and Some Applications. *Proc. IEEE* **1991**, *3*, 278–305. [[CrossRef](#)]
27. Gradshteyn, I.S.; Ryzhik, I.M. *Table of Integrals, Series, and Products*, 5th ed.; Academic Press: London, UK, 1994.
28. Papoulis, A.; Pillai, S.U. *Probability, Random Variables and Stochastic Processes*, 4th ed.; McGraw-Hill, Inc.: New York, NY, USA, 2002.
29. Tokgoz, Y.; Rao, B.D. Performance Analysis of Maximum Ratio Transmission Based Multi-Cellular MIMO Systems. *IEEE Trans. Wirel. Commun.* **2006**, *1*, 83–89. [[CrossRef](#)]
30. Pham, H. *Handbook of Engineering Statistics*; Springer: New York, NY, USA, 2006.
31. Zhang, J.; Kountouris, M.; Andrews, J.G.; Heath, R.W. Multi-Mode Transmission for the MIMO Broadcast Channel with Imperfect Channel State Information. *IEEE Trans. Commun.* **2011**, *3*, 803–814. [[CrossRef](#)]
32. Kim, T.; Min, K.; Jung, M.; Choi, S. Scaling Laws of Optimal Training Lengths for TDD Massive MIMO Systems. *IEEE Trans. Veh. Technol.* **2018**, *8*, 7128–7142. [[CrossRef](#)]

33. Kim, Y.; Miao, G.; Hwang, T. Energy Efficient Pilot and Link Adaptation for Mobile Users in TDD Multi-User MIMO Systems. *IEEE Trans. Wirel. Commun.* **2014**, *1*, 382–393. [[CrossRef](#)]
34. 3GPP Technical Specification TS 38.214. NR; Physical Layer Procedures for Data. Available online: <https://www.3gpp.org/dynareport/38214.htm> (accessed on 20 July 2020).



© 2020 by the authors. Licensee MDPI, Basel, Switzerland. This article is an open access article distributed under the terms and conditions of the Creative Commons Attribution (CC BY) license (<http://creativecommons.org/licenses/by/4.0/>).